Molecular Dynamics Simulation of $[Gd(egta)(H_2O)]^-$ in Aqueous Solution: Internal Motions of the Poly(amino carboxylate) and Water Ligands, and Rotational Correlation Times

Fabrice Yerly,[a] Kenneth I. Hardcastle,[b] Lothar Helm,[a] Silvio Aime,[c] Mauro Botta,[d] and André E. Merbach*[a]

Abstract: Molecular dynamics simulations of $[Gd(egta)(H_2O)]^-$ ($egta^{4-}$ = 3,12-bis(carboxymethyl)-6,9-dioxa-3,12-diazatetradecanedioate(4 −)) have been performed without any artificial constraint on the first coordination sphere, such as covalent bonds between the Gd^{3+} and the coordination sites. Two new crystallographic structures were determined for this gadolinium chelate and used to start two molecular dynamics simulations. $[Gd(egta)(H_2O)]^-$ and $[Gd(egta)]^-$ were both observed during the simulations, with a mean volume for the reaction of dissociation $[Gd(egta)(H_2O)]^- \rightarrow [Gd(egta)]^- + H_2O$ of $+7.2\,cm^3\,mol^{-1}$, which corroborates the previously published experimental value of $+10.5\,cm^3\,mol^{-1}$. Changes in the conformation of the complex with the inversion of several dihedral angles are observed in the simulations independently from the water dissociation. Very fast changes of the third-order rotation axis direction of the Gd^{3+} coordination polyhedron (of symmetry D_{3h}) are observed during the simulations and are related to the mechanism of electronic relaxation of the complex. Different rotational correlation times (τ_R) were calculated from the simulations on various observables of the complex. Protons of the inner sphere have different τ_R. The mean τ_R of the two Gd–HW (HW = hydrogen of water molecule) vectors is 72% lower than τ_R of the complex, and 75% lower than τ_R of the vector Gd–OW (OW = oxygen of water molecule). This discrimination of the tumbling rates should be taken into account in future global ^{17}O NMR, EPR and NMRD (nuclear magnetic relaxation dispersion) data analysis.

Keywords: conformation analysis · gadolinium · imaging agents · magnetic resonance imaging · molecular dynamics · solvation

Introduction

Poly(amino carboxylate) ligands are widely used to form complexes with lanthanide(III) ions. A major application of these compounds is the use of gadolinium(III) complexes as magnetic resonance imaging (MRI) contrast agents, due to the ability of the high electronic spin of Gd^{3+} S = 7/2 to enhance the water proton relaxation rate. This property, called *relaxivity*, is commonly divided into two contributions: inner sphere relaxivity is due to protons of the water molecules that directly coordinate the metal ion and that exchange chemically with the bulk, and outer sphere relaxivity, due to dipolar interactions through space with surrounding water molecules.[1, 2] A previous multinuclear NMR study of various lanthanide complexes with the poly(amino carboxylate) ligand $egta^{4-}$ showed that the chemical water exchange rate on $[Gd(egta)(H_2O)]^-$, of $3.1 \times 10^7\,s^{-1}$, was one order of magnitude higher than on $[Gd(dota)(H_2O)]^-$ (dota = 1,4,7,10-pentakis(carboxymethyl)-1,4,7,10-tetraazacyclododecane) or on $[Gd(dtpa)(H_2O)]^{2-}$ (dtpa = 1,1,4,7,7-pentakis(carboxymethyl)-1,4,7-triazaheptane), with values of $3.1 \times 10^6\,s^{-1}$ and $4.1 \times 10^6\,s^{-1}$ respectively.[3] From new crystallographic structural data and molecular dynamics simulation, this study attempts to understand what happens in solution in the first coordination sphere, how intramolecular motions can influence the water exchange, and the reasons for the high water

[a] Prof. A. E. Merbach, F. Yerly, Dr. L. Helm
Institute of Inorganic and Analytical Chemistry
EPFL-BCH
1015 Lausanne (Switzerland)
Fax: (+41) 21-693-98-75
E-mail: andre.merbach@epfl.ch

[b] Prof. K. I. Hardcastle
Department of Chemistry, Emory University
Atlanta, G.A. 30322-2210 (USA)

[c] Prof. S. Aime
Dipartimento di Chimica Inorganica
Università degli Studi di Torino
Via P. Giura 7, 10125 Torino (Italy)

[d] Prof. M. Botta
Università del Piemonte Orientale "Amedo Avogadro"
Corso Borsalino 54, 15100 Alessandria (Italy)

Supporting information for this article is available on the WWW under http://www.wiley-vch.de/home/chemistry/ or from the author.

  0947-6539/02/0805-1031 $ 17.50+.50/0

exchange rate of $[Gd(egta)(H_2O)]^-$. Molecular dynamics simulations also gives us a new insight into the mechanisms responsible for the electron spin relaxation of such complexes.

Experimental Section

X-ray experiment: A suitable crystal of $Na[Gd(egta)\cdot 4.5\,H_2O]$ was coated with Paratone N oil, placed on the end of a silica fiber and mounted in a goniometer head on a Nonius CAD4 diffractometer in a stream of cold nitrogen gas. The crystal was centered optically. Unit cell parameters and an orientation matrix for data collection were obtained at $-75\,^{\circ}C$ by using the centering program in the CAD4 system. Selected bond lengths for $[Gd(egta)(H_2O)]^-$ from this study and other Gd^{3+} complexes are listed in Table 1. Crystallographic acquisition parameters are available in the Supporting Information and atomic coordinates are available from the Cambridge Crystallographic Data Cetnre (see below).

The actual scan range was calculated by scan width = scan range + $0.35\tan\theta$, and backgrounds were measured by using the moving-crystal/moving-counter technique at the beginning and end of each scan. Two representative reflections were monitored every 2 h as a check on instrument and crystal stability. Lorentz, polarization, and decay corrections were applied to the data as well as an absorption correction based on a series of ψ scans.

The structure was solved by Direct Methods by using SHELXTL/PC V5.03;[8] this revealed positions for most of the non-hydrogen atoms. All other non-hydrogen atoms were found by successive difference Fourier syntheses, including the water molecules. Hydrogen atoms on the egta ligand were placed in their expected chemical positions using the HFIX command in SHELXTL and included as riding atoms in the final cycles of least squares. Due to the relatively poor crystallinity of the crystal, disorder of the solvent waters and subsequent fall off of intensity with $\sin\theta$, the hydrogen atoms attached to the water were not found or included in the final structure. Only the gadolinium and sodium atoms could be refined anisotropically in the final cycles of least squares.

Neutral atom scattering factors and values of $\delta f'$ and $\delta f''$ were taken from reference [9]. Structure refinement and preparation of figures and tables for publication were carried out on PC's with SHELXTL/PC. Crystallographic data (excluding structure factors) for the structures reported in this paper have been deposited with the Cambridge Crystallographic Data Centre as supplementary publication no. CCDC-169081. Copies of the data can be obtained free of charge on application to CCDC, 12 Union Road, Cambridge CB2 1EZ, UK (fax: (+44) 1223-336-033; e-mail: deposit@ccdc.cam.ac.uk).

Computational Methods

Molecular dynamic simulations were performed on a SGI Origin 200 by using the program AMBER 6.0.[10] The Amber force field[11] was used for all atoms. The σ and ε van der Waals parameters for Gd^{3+} were chosen to reproduce experimental coordination of the metal complexed in solution by two nitrogen and six oxygen atoms of the $egta^{4-}$ ligand, and by one oxygen from the inner sphere water molecule. We assigned values of 3.207 Å and 0.20 kcal mol^{-1} for σ_{ii} and ε_{ii} of Gd^{3+}, respectively. Atomic charges were calculated on all solute atoms at the RHF level by the Mulliken method with the program Gaussian 98[12] with a 6-31G** basis set.

Two different molecular structures were observed in the unit cell, called molecules A and B, with one water molecule coordinating to Gd^{3+} in molecule A. Averaged atomic charges calculated on both molecules A and B are presented in Table 2. We assume that Mulliken charges better describe interactions in the complex than MEP methods such as Merz–Kollmann,[13] developed to reproduce the external potential. Calculations were carried out on Gd^{3+} with all 4f electrons frozen, by means of the effective core potential of Dolg et al.[14] In agreement with a previous study,[15] we found that the metal ion chelated by a multidentate ligand is better described within the classical molecular mechanics framework with an atomic charge of 3.0, even if ab initio calculations allow some electron transfer onto Gd^{3+}. This was applied to structures A and B, leading two sets of charges.

Preliminary simulations performed on both structures with the two sets of charges showed that atomic charges calculated for structure B better describe the behavior in solution of the complex, for example, the coordination number of the metal or stability of the complex. The XR-B (XR = X-ray) charge set was used for the final simulations, and the OWC and HWC (for definitions of OWC and HWC see Table 2) charges calculated on structure A were used to describe the polarization of the coordinated water molecule.

Table 2. Atomic charges derived from ab initio calculations on structures A and B.

	Atom type	XR-A	XR-B
Gd	Gd	+3.000	+3.000
OB	O carboxylate (bound)	−0.869	−0.944
OF	O carboxylate (free)	−0.744	−0.718
CO	C carboxylate	+0.780	+0.820
CN	C methylene	−0.053	−0.056
HN	H methylene	+0.137	+0.138
N	N amine	−0.970	−0.944
C	N N-ethylene bridge	−0.020	−0.016
H	H N-ethylene bridge	+0.139	+0.138
C	C O-ethylene bridge	+0.107	+0.118
H	H O-ethylene bridge	+0.135	+0.152
OE	O ether	−0.857	−0.908
CE	C ether ethylene bridge	+0.105	+0.098
HE	H ether ethylene bridge	+0.149	+0.155
OWC	O inner sphere water	−1.050	–
HWC	H inner sphere water	+0.525	–

Starting structures, that is, A and B X-ray structures, were placed in a $30\times 30\times 50$ Å^3 box of the TIP3P Jorgensen water model.[16] For structure B, the atom OF4(A) was replaced by a water molecule placed at 2.53 Å from Gd^{3+}. An Na^+ ion was initially placed at 20 Å of the Gd^{3+}, to warrant a neutral global charge without interacting with the complex. Van der Waals interactions were calculated following the Lennard–Jones 6–12 potentials. Particle Mesh Ewald (PME) was used to calculate energy with a grid density of one point per Å^3. After a 1000 steps energy minimization of the system, a simulation of 30 ps was performed with the frozen complex to equilibrate the water bath. Simulation parameters are summarized in Table 3.

Simulation trajectory files were analyzed by using the KERUBIN program[17] to calculate radial distribution functions, distances, and dihedral angles. Solid angles, rotational correlation functions, and internal basis

Table 1. Selected distances [Å] between atoms[a] in Gd^{3+} complexes as found by X-ray crystallography.

	$[Gd(egta)(H_2O)]^-$ This work	$[Gd(dtpa)(H_2O)]^{2-}$ Ref. [4]	$[Gd(dota)(H2O)]^-$ Ref. [4]	$[Gd(ttha)]^{3-}$ Ref. [4]	$[Gd(N_3O_6\text{-L2})]$[b] Ref. [4]
Gd–OB	2.35(3)	2.39	2.37	2.39	2.33
Gd–OF	4.37(3)	4.41	4.44	4.44	4.41
Gd–N	2.57(5)	2.68	2.66	2.67	2.66
Gd–OE	2.50(3)	–	–	–	2.53
Gd–OWC	2.53(2)	2.44	2.46	–	–

[a] Atom types refer to definitions in Table 2. [b] 1,7,13-Triaza-4,10,16-trioxa-*N*,*N*′,*N*″-triscarboxymethylcyclooctadecane Gd^{3+} complex.

0947-6539/02/0805-1032 $ 17.50+.50/0 *Chem. Eur. J.* **2002**, *8*, No. 5

Table 3. Overview of simulation parameters for $[Gd(egta)(H_2O)]^-$.

	MD-A	MD-B
starting structure	XR-A	XR-B
number of water molecules	1364	1345
equilibration time [ps]	30	30
simulation time [ps]	1000	1000
stored configurations	5000	5000
τ_T [ps][a]	0.5	0.5
τ_P [ps][a]	0.2	0.2
average density [g cm^3]	1.0377324	1.0377417
temperature [K]	300	300
pressure [atm]	0.986	0.986
van der Waals cutoff [Å]	8.0	8.0
grid density for PME [Å^{-3}]	1.0	1.0

[a] Relaxation times for temperature and pressure in the algorithm of Berendsen.

cartesian/polar coordinates were calculated by using a custom program running on the Matlab environment.[18] All plots, statistical properties measures, and least square calculations were carried out with the VISUALISEUR program, running on Matlab.[19a,b] Connolly surfaces and volumes[20] were computed with the CERIUS^2[21] package, with a grid density of 64 points per Å^3, and a probe radius of 1.4 Å.

Results and Discussion

X-ray measurements: The unit cell contains two different molecules of the complex of Gd^{3+} with the ligand $egta^{4-}$ in the asymmetric unit: molecule A has one water in the inner sphere coordinating the Gd^{3+}; in molecule B the position which could have been occupied by a bound water molecule is occupied by a carboxyl oxygen donated from molecule A (OF4(A), see Figure 1).

The primary difference in the two molecules, aside from the bound water molecule, is in the conformation of one ethylene bridge, OE2-C3-C4-N2. In molecule A, the C3–C4 bond is almost perpendicular to the OB4, OE2, OE1, OB1 plane, whereas in molecule B this bond is at a much less steep angle, almost parallel, to the corresponding plane. A stereochemical description of the structure of the complex can be described as dihedral conformation suite I-II-III-IV, V-VI-VII (see Scheme 1). This leads to a $\delta\delta\delta\lambda\lambda\lambda\lambda$ conformation for molecule A, and to a $\delta\delta\delta\lambda\,\delta\lambda\lambda$ conformation for molecule B.

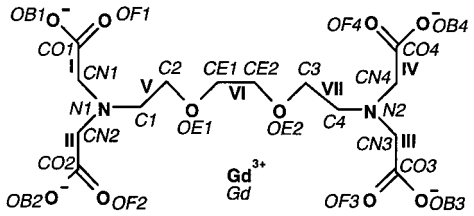

Scheme 1. A schematic diagram of the ligand indicating the dihedral conformation suite I-II-III-IV and V-VI-VII.

Averaged distances between Gd and the coordination sites in $[Gd(egta)(H_2O)]^-$ and some other selected complexes are presented in Table 1 (for definitions of atom types see Table 2), as determined by solid state crystallography. Carboxylate oxygens and amine nitrogens are slightly closer to Gd^{3+} in the $egta^{4-}$ complex than in the $dtpa^{5-}$, $dota^{4-}$, and $ttha^{6-}$ complexes. However, Gd–OW in $[Gd(egta)(H_2O)]^-$ is about 3% longer than in the $[Gd(dtpa)(H_2O)]^{2-}$ and $[Gd(dota)]^-$ complexes. The chemical water exchange follows a dissociative D mechanism, which has a very important consequence for the water chemical exchange rate. The dissociation energy of the Gd–OW bond decreases when its length increases, implying a decrease of the energetic cost for the exchange. This is the reason why the water chemical exchange rate on $[Gd(egta)(H_2O)]^-$ is ten times higher than on $[Gd(dtpa)(H_2O)]^{2-}$. This raises the question of why the Gd–OW distance is greater in the $egta^{4-}$ complex?

Molecular dynamics simulations

Water departure: In both the molecular dynamic simulations of molecules A and B (MD-A and MD-B, respectively), the starting structures consisted of the hydrated form of the complex. The inner sphere water molecule was polarized by using atomic charges of −1.050 and 0.525 for oxygen and hydrogen respectively (see Table 2), instead of the −0.834 and 0.417 TIP3P charges.[16] After 457 ps for MD-A and 132 ps for MD-B, the inner sphere water molecule left the complex, and was not replaced by an other one during the 1000 ps simulations (Figure 2). After the water molecule had left the complex, its polarization was removed and TIP3P charges were imposed. No gradual polarization of the water molecules approaching the complex was allowed in

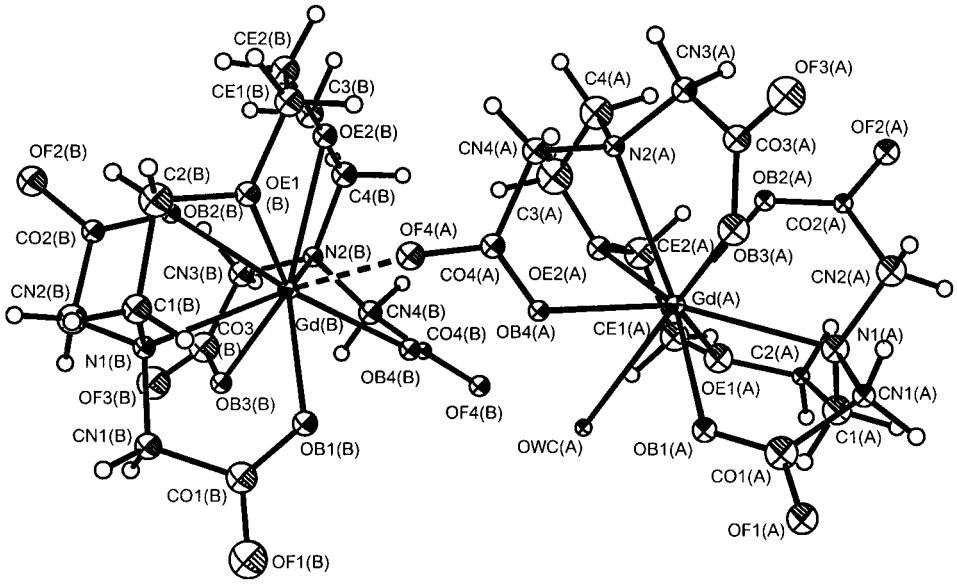

Figure 1. Structures and intermolecular interaction between molecules A and B, as determined in the solid state by X-ray crystallography.

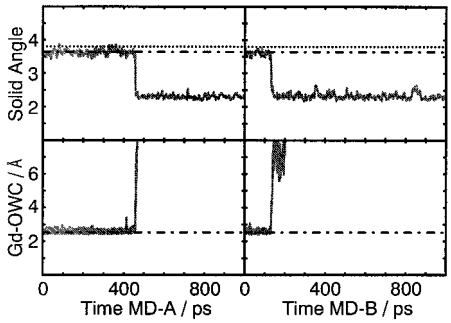

Figure 2. Top: Time dependence of the solid angle defined by the four ligand atoms surrounding the coordinated water molecule: OE1, OE2, OB4, OB1 and the Gd^{3+} ion. Bottom: Time dependence of the distance Gd–OWC. Left: MD-A simulation, right: MD-B simulation. MD simulation = solid gray line, XR-A value = dashed dotted line, XR-B value = dotted line.

the simulations; this explains why the complex remains eight-coordinate after the removal of the water. From the ^{17}O NMR data analysis a ^{17}O hyperfine coupling constant of -3.2×10^6 rad s^{-1} was obtained, implying that the complex has one water molecule in the inner sphere.[3] At the beginning of both simulations, the Gd^{3+} ion was coordinated by nine donor atoms: six oxygen and two nitrogen atoms from the egta^{4-} ligand, and one oxygen atom from the coordinated water molecule. We label these initial parts MD-A9 and MD-B9 for simulation MD-A and MD-B, respectively. After the departure of the water molecule, the Gd^{3+} ion is coordinated by 8 donor atoms(6 O and 2 N from the egta^{4-}). These final parts are labeled MD-A8 and MD-B8 for simulation MD-A and MD-B, respectively. In MD-A9 and MD-B9, the coordination number of the metal ion is nine as observed experimentally, with one water molecule in the first coordination shell. In MD-A8 and MD-B8, the structures correspond to what could be the intermediate in the dissociative water exchange. In the initial complex the water molecule occupies a face of the coordination polyhedron that is defined by the atoms OE1, OE2, OB4, and OB1. The solid angle defined in Figure 2 describes the degree of opening of that face. When the inner sphere water molecule leaves the complex, this angle decreases from 3.6 to 2.3 steradian (MD-A). The mean solid angle for the face determined by the atoms OE1, OE2, OB3, and OB2 (the other face which is in principle able to receive a water molecule) is unchanged, taking values of 2.4 and 2.3 steradian before and after the departure of the water molecule (MD-A). The same values obtained for the solid angles of the two faces in the eight-coordinate complex implies the equivalence of both sites for an incoming water molecule.

Solution structure of the chelate: Averaged Gd–coordination site distances from simulated solutions and from solid state X-ray are presented in Table 4. In most cases, the distances appear to be longer in simulated solution than in the solid state, due to the solvation effect that is present only in simulations. Distances between the metal ion and the ligand donor atoms are generally shorter when the water molecule is gone than when the metal is hydrated, due to a decreased steric repulsion. Note that distances Gd–N1 and Gd–N2 are significantly different in the solid state and that this difference disappears in solution. This is probably due to higher internal ligand constraints in the solid state caused by the contraction of the Gd^{3+} coordination sphere.

Table 4. Selected distances [Å] in [Gd(egta)]$^-$ in solid-state structures and from simulations in solution.

XR-A	XR-B	MD-A9	MD-B9	MD-A8	MD-B8	
Gd–OB1	2.35	2.25	2.49	2.50	2.45	2.45
Gd–OB2	2.37	2.36	2.51	2.51	2.45	2.45
Gd–OB3	2.30	2.29	2.50	2.49	2.45	2.45
Gd–OB4	2.42	2.43	2.51	2.52	2.45	2.45
average	*2.36(2)*	*2.33(2)*	*2.50(7)*	*2.51(7)*	*2.45(5)*	*2.45(5)*
Gd–OE1	2.51	2.48	2.45	2.45	2.43	2.42
Gd–OE2	2.54	2.48	2.47	2.47	2.43	2.43
average	*2.52(2)*	*2.48(2)*	*2.46(6)*	*2.46(6)*	*2.43(5)*	*2.43(5)*
Gd–N1	2.50	2.54	2.59	2.58	2.53	2.53
Gd–N2	2.56	2.67	2.59	2.60	2.53	2.53
average	*2.53(2)*	*2.60(2)*	*2.59(6)*	*2.59(7)*	*2.53(5)*	*2.53(5)*
Gd–OF1	4.38	4.29	4.46	4.46	4.35	4.39
Gd–OF2	4.44	4.39	4.44	4.45	4.29	4.31
Gd–OF3	4.17	4.35	4.45	4.46	4.33	4.34
Gd–OF4	4.47	4.45	4.45	4.46	4.29	4.30
average	*4.37(2)*	*4.37(2)*	*4.45(12)*	*4.46(12)*	*4.31(15)*	*4.32(15)*
Gd–OWC	2.53(2)		2.58(9)	2.59(8)		
Gd–1HWC			3.25	3.26		
Gd–2HWC			3.27	3.25		
average			*3.26(18)*	*3.26(19)*		

There is no significant difference between dihedral angles values in solid state and in simulated solution when the complex is hydrated, as can be seen in Table 5. During the simulations, some dihedral angles change sign, indicating a conformation change. An exchange involving such a dihedral angle change for the OE-C-C-OE bridge has been observed on the NMR timescale in a previous paper for various lanthanide(III) egta^{4-} complexes, including [Eu(egta)-(H_2O)]$^-$.[3] Figure 3 summarizes the changes in conformation of the ligand and Table 6 lists the different events that occur during the simulation and also the stereochemical structure of the complex following those changes by describing the conformation of the dihedral angle suite I-II-III-IV (acetyl), V-VI-VII (bridge) as defined on Scheme 1.

Table 5. Selected dihedral angles [°] in [Gd(egta)]$^-$ in solid-state structures and from simulations in solution.

	XR-A	XR-B	MD-A9[a]	MD-B9[a]	MD-A8[a]	MD-B8[a]
OE1-C-C-OE2	−48	−52	−48(9)	−48(10)	+51(9)	+53(8)
OE1-C-C-N1	−52	+58	−54(7)	+50(9)	−54(7)	−54(7)
OE1-C-C-N2	−61	−63	−47(10)	−49(9)	−54(7)	−54(8)
N1-C-C-OB1	+27	+31	+24(20)	+23(18)	+17(18)	+19(18)
N1-C-C-OB2	−21	−20	−22(19)	−22(21)	−29(15)	−25(17)
N2-C-C-OB3	+42	+13	+13(19)	+20(19)	+21(15)	+18(17)
N2-C-C-OB4	+20	+15	+22(14)	+19(13)	−29(14)	−28(16)

[a] Averages on the major conformation. Standard deviations are in parentheses.

Volume profile for the reaction $[Gd(egta)(H_2O)]^- \rightarrow [Gd(egta)]^- + H_2O$: In both simulations, Connolly volumes have been calculated for 250 equally spaced configurations

0947-6539/02/0805-1034 $ 17.50+.50/0 *Chem. Eur. J.* **2002**, *8*, No. 5

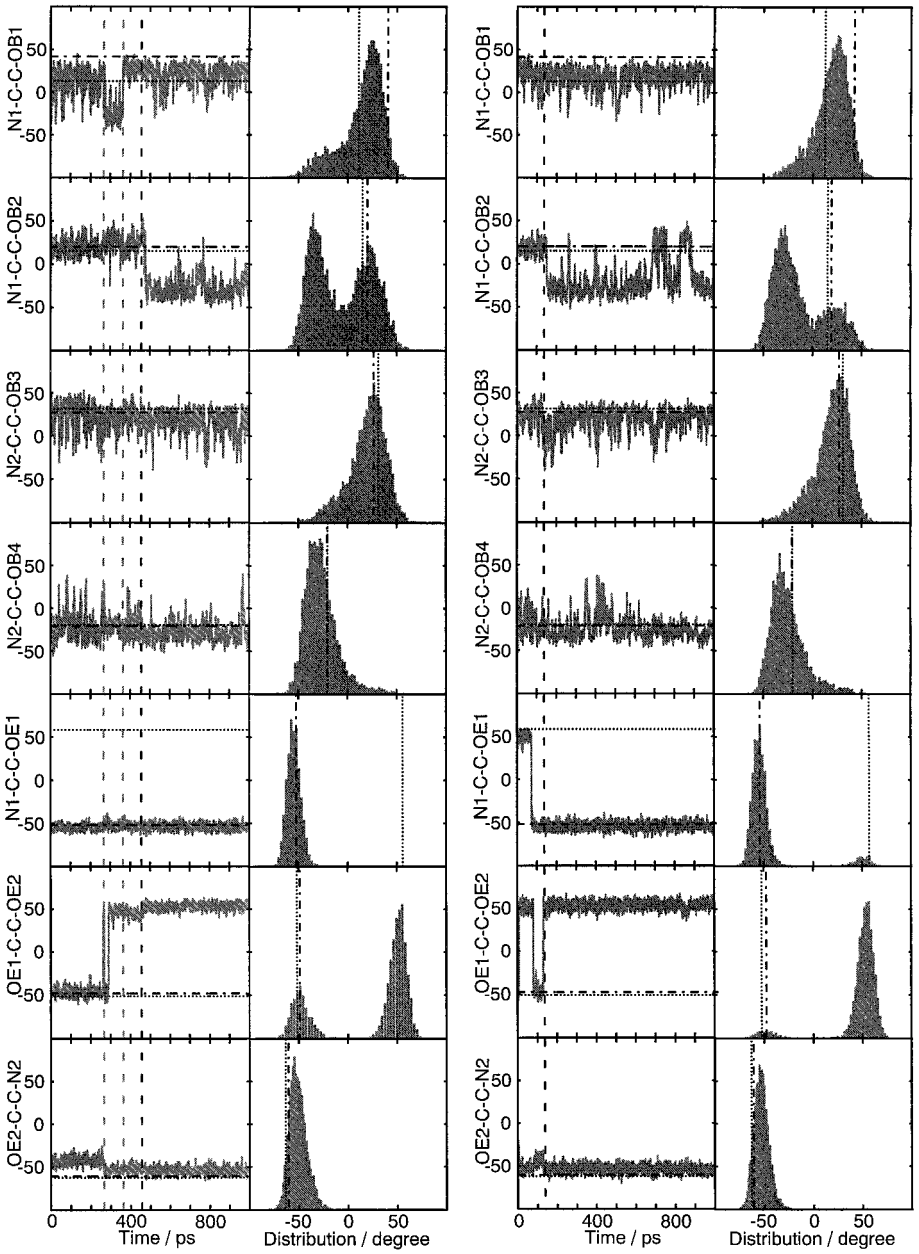

Figure 3. Time evolution of selected dihedral angles in the ligand egta^{4-} during simulation, MD-A (left) and MD-B (right), and their respective distributions. MD value = solid gray line, XR-A structure = dashed dotted line, XR-B structure = dotted line. Vertical gray dashed lines mark the following events in MD-A (in chronological order): 1) the OE1-C-C-OE2 and N1-C-C-OB1 flips, 2) the N1-C-C-OB1 back flip. Vertical black dashed lines mark the departure of the coordinated water molecule.

(see Figure 4). Before departure of the coordinated water molecule, the molecular volume is taken as the Connolly volume of $[Gd(egta)(H_2O)]^-$. After departure of the water molecule, the molecular volume is taken as the Connolly volume of $[Gd(egta)] + V_{H_2O}$, with $V_{H_2O} = 18.07\ cm^3\,mol^{-1}$. This method has been described by Kowall et al.[22] The difference between the nonhydrated and hydrated forms of the complex should give the volume of reaction. Results obtained from both simulations are smaller by about $3\ cm^3\,mol^{-1}$ than the experimental fitted value (see Table 7). The origin of this underestimation is most likely due to the fact that we did not take into account the volume variation of the second sphere, a change that is difficult to define precisely. The experimental value of $+10.5\ cm^3\,mol^{-1}$ describes a macroscopic phenomenon that includes water rearrangement and electrostriction of the leaving water molecule. The calculated value represents the variation in the volume of a more precise system, that is, the complex plus a water molecule. It is possible that this difference of $3\ cm^3\,mol^{-1}$ represents a solvent contribution and leads us to believe that the nonhydrated form of the complex observed in simulations represents a realistic intermediate for the water exchange reaction.

Table 6. Summary of the different conformations appearing in simulations MD-A and MD-B, and events that caused the situation.

	Case/period [ps]	Conformation	Cause of the situation
XR	A	δδδλλλλ	solid state
	B	δδδλδλλ	solid state
MD-A	0–266	δδδλλλλ	first period of simulation
	266–364	λδδλλδλ	OE1-C-C-OE2 and N1-C-C-OB1 flips
	364–457	δδδλλδλ	N1-C-C-OB1 back flip at 364 ps
	457–1000	δλδλλδλ	departure of the water molecule
MD-B	0–7	δδδλδλλ	first period of simulation
	7–77	δδδλδδλ	OE1-C-C-OE2 flip at 7 ps
	77–132	δδδλλλλ	OE1-C-C-OE2 back flip N1-C-C-OE1 flip
	132–1000	δλδλλδλ	departure of the water molecule

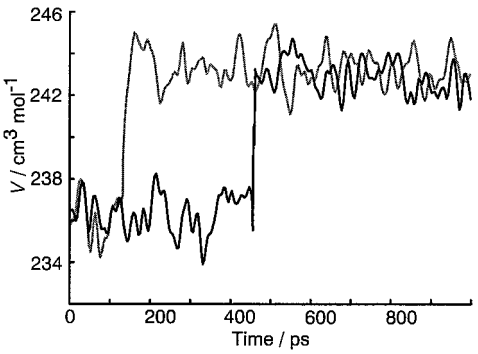

Figure 4. Connolly volume profile of the complex as a function of time for MD-A (black line) and MD-B (gray line).

Table 7. Averages of molecular volumes [cm^3mol^{-1}] calculated from the Connolly volumes.

	MD-A	MD-B	Exptl[3]
$[Gd(egta)(H_2O)]^-$	+236.1	+235.8	–
$[Gd(egta)]^-$	+243.0	+243.3	–
$\Delta V(9 \rightarrow 8)$	+6.9	+7.5	$+10.5 \pm 1.0$

Description of the solvation: The radial distribution functions of water around Gd^{3+} before and after departure of the inner sphere water molecule for both simulations, MD-A and MD-B, are presented in Figure 5. There is no significant difference in $g(r)$ between MD-A and MD-B. However, in MD-B, H_2O has already left the complex at 132 ps. Consequently we use

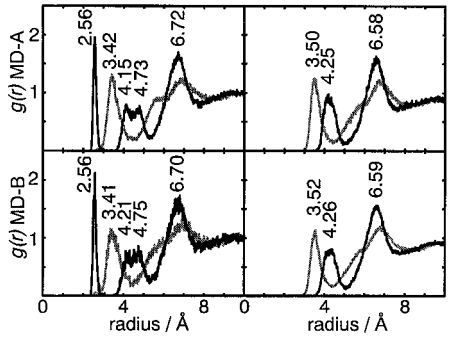

Figure 5. Radial distribution functions $g(r)$ of the water oxygen (black line) and hydrogen (gray line) atoms around Gd^{3+} in simulation, MD-A (top) and MD-B (bottom). $g(r)$ on the left-hand side describes the bulk water distribution around the hydrated form of the complex $[Gd(egta)(H_2O)]^-$. The right-hand side describes the solvent distribution when the inner sphere water molecule has left.

only $g(r)$ calculated from MD-A. Integration of $g(r)$ gives 7.0 and 5.3 water molecules in the second hydration shell for MD-A9 and MD-A8, respectively. This loss of two second-shell water molecules with the departure of the inner sphere water molecule is due to the diminution of the space directly accessible to the second-shell water, as described by the decrease of the solid angle defined in Figure 2. About half the protons of the second shell appear to be closer (3.42 Å) to Gd^{3+} than the water oxygens (4.15, 4.73 Å). Integration of $g(r)$ gives 7.8 (MD-A9) and 6.3 (MD-A8) protons of the second shell that are closer to the metal ion than oxygens. This means that one of the second-shell water protons points towards a negatively charged ligand atom (OE, OF, and OB), and the other one, farther than 4.7 Å, interacts with bulk water molecules. Local organization of the second-shell water molecules has been observed by molecular dynamics simulations for several similar complexes, and used to calculate the outer sphere relaxivity.[15] In MD-A9, $g(r)$ shows a split of the second-shell oxygen atoms at 4.15 and 4.73 Å instead of a single peak at 4.25 Å for the eight-coordinate form of the complex (MD-A8). This can be explained as follows: a water molecule in the inner sphere can be localized in one of the two faces delimited by OE1, OE2, OB4, and OB1 or by OE1, OE2, OB3, and OB2 (See Scheme 1). When a water molecule is bound to Gd^{3+} (MD-A9), the two faces have different shapes, and the water molecules that are close to the nonhydrated face can come closer to Gd^{3+} than the ones near the hydrated face. When the complex has no water molecule in the inner sphere (MD-A8), the two faces become equivalent, and the accessibility of the complex for the second-shell water is the same. The distance of the second-shell water oxygen atoms from Gd^{3+} has similar values for both faces in MD-A8 (4.25 Å) and the nonhydrated face in MD-A9 (4.15 Å). The same similarity is observed for the solid angles of these faces, as described in the section about water departure.

Symmetry analysis: Nine coordination sites around a metal ion can adopt one of the two approached symmetries: D_{3h} if a tricapped trigonal prism is formed, or C_{4v} for a monocapped square antiprism.[23] In solution, vibrations cause distortion of the coordination polyhedron and this decreases the symmetry. An algorithm has been developed to find, for a given coordination polyhedron, the nearest tricapped trigonal prism and the nearest monocapped square antiprism, at each time step. Details of the algorithm used can be found in the Supporting Information. Searching for C_{4v} symmetry gave poor results; there is very little correlation between symmetries from one time step to the next. For example the best C_4 rotation axis changes statistically every 0.31 ps, which is close to the time step of 0.20 ps between two stored frames. More than 300 best-fitting C_{4v} structures were observed during simulation, and no single one appeared more than 90 times. Searching for D_{3h} symmetry gave better results in both simulations. In MD-A and MD-B, three different polyhedra were found. Polyhedron S1 has the two nitrogen atoms and the water oxygen in a capping positions. Polhedrons S2 and S3 have one ether ogygen, one nitorgen, and one carboxylate oxygen atoms in the capping positions. In S2, the capping positions are occupied by OE2, N1, and OB4. In S3, the capping positions are occupied by OE1, N2, and OB1. Table 8 summarizes the results of the D_{3h} symmetry analyses during the different periods of simulations P1, P2, and P3. During P1 the complex is in the $\delta\delta\delta\lambda\lambda\lambda$ conformation, during P2 in the $\lambda\delta\delta\lambda\lambda\delta\lambda$, conformation and during P3 in the $\delta\delta\delta\lambda\lambda\delta\lambda$ conformation. The three D_{3h} polyhedra are defined only by the arrangement of the nine coordination sites around Gd^{3+} and do not describe the complete stereochemical conformation of the whole complex. The three polyhedra found in MD-A in the different conformations are represented in Figure 6. Polyhedron S1 is found in both X-ray solid-state structures and in all observed conformations in simulated solution. Nevertheless, in solution this polyhedron with the water

Table 8. Populations of the various polyhedra S1, S2, and S3 in the different conformations.

	Case/period [ps]	S1 [%]	S2 [%]	S3 [%]
X-ray	A structure	100	0	0
	B structure	100	0	0
MD-A	0–266	7	93	0
	266–364	23	0	77
	364–457	5	95	0
MD-B	0–7	8	92	0
	7–77	10	90	0
	77–132	10	90	0

0947-6539/02/0805-1036 $ 17.50+.50/0 *Chem. Eur. J.* **2002**, *8*, No. 5

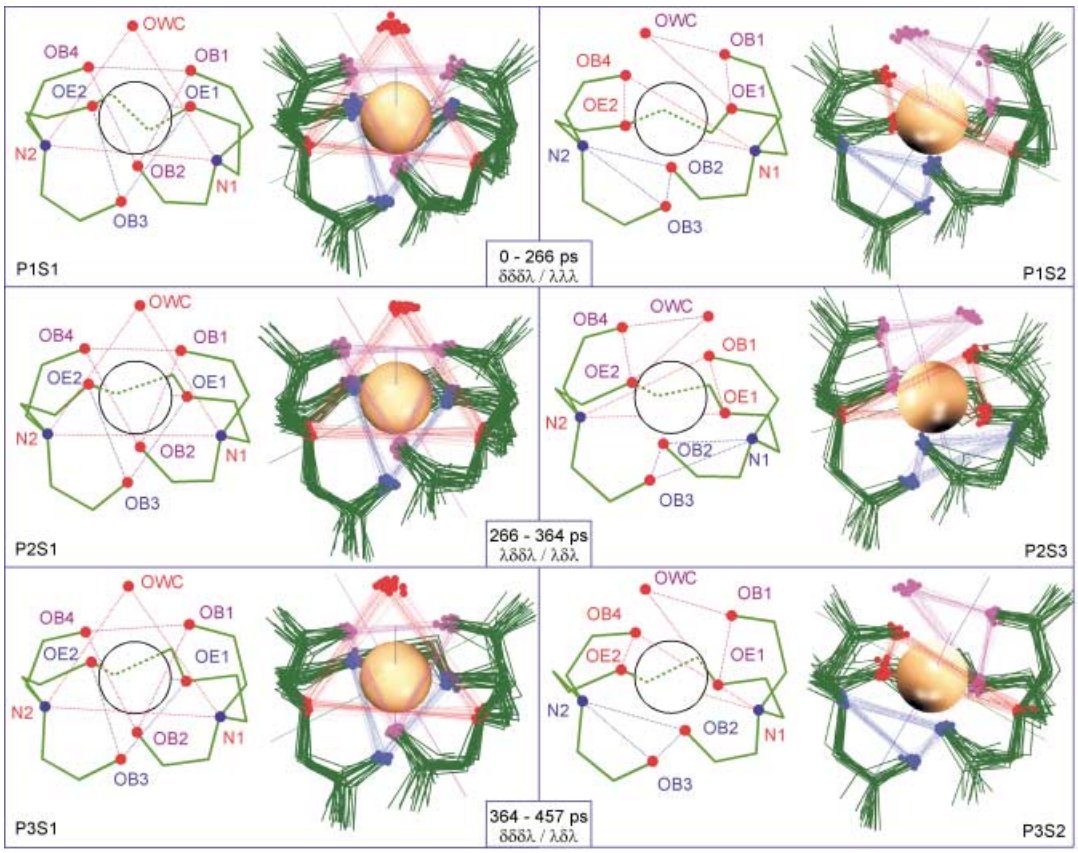

Figure 6. Representation of the three conformations of the complex in MD-A observed while it has one inner sphere water molecule, and identified D_{3h} polyhedra labeled S1, S2, and S3. Ligand = green line, capping positions = red circles, prismatic positions = blue and purple circles. In each cell, the left part is schematic while the right part is a superposition of 20 frames of simulation.

molecule in capping position happens rarely. Schauer et al. have observed polyhedron S1 for $[Er(egta)(H_2O)]^-$ in the solid state by crystallography.[24] A coalescence of some ^1H and ^{13}C NMR signals led Aime et al. to propose that for $[Ln(egta)(H_2O)]^-$, with $Ln^{3+} = Eu^{3+}$ to Er^{3+}, there is a equilibrium between two different D_{3h} polyhedra.[3] Their equilibrium involved an exchange of the positions of two carboxylate oxygens. In our case, the changes are only due to small sliding of the positions of the atoms, involving a lower activation energy. However symmetry reorientations observed in our simulations occur on the picosecond timescale, whereas the proposed equilibration occurs on the milisecond timescale. In polyhedron S1, the water molecule is centered between the neighboring atoms OE1, OE2, OB4, and OB1. In polyhedra S2 and S3, the inner sphere water molecule is no longer centered. In S2 the water molecule is localized near the atoms OB4 and OE2 and in S3 it is near the atoms OB1 and OE1. This motion of the coordinating water molecule following conformational changes of the complex can be seen in Figure 7. On the left hand side of the figure the gray zones are composed of S1 and S2 polyhedra (periods P1 and P2) and the black zones by S1 and S3 polyhedra (period P2). S1 is the intermediate region in which the water oxygen is at the same distance from both nitrogen atoms, leading a capping behavior. On the right hand side, the inner sphere water molecule has left, and the surrounding coordination sites come closer to each other; this can also be observed in

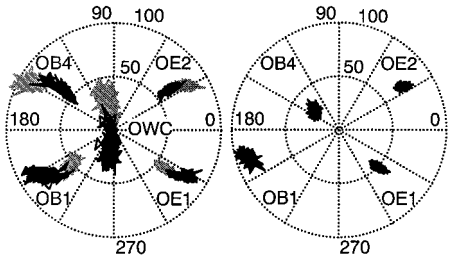

Figure 7. Angular projection of the hydrated side of the complex before (left) and after (right) departure of the water molecule from the first shell in simulation MD-A. On the left-hand side, the gray zones correspond to periods where N1-C-C-O1 has δ conformation (0–266 ps and 364–457 ps), and black zones where it has λ conformation (266–364 ps).

Figure 2, with the decrease of the solid angle described by the spherical area OB1, OE1, OE2, and OB4, with the sphere centered on Gd^{3+} as previously discussed in the section about the water departure. A flip from one polyhedron to an other one happens statistically every 2.2 ps, which is extremely fast (one event every 11 time steps). This has two consequences; the first one is that there is no way to observe such a rearrangement by NMR spectroscopy, which only measures the time-averaged structures of S1, S2, and S3. The second consequence is that the energy associated with such changes is very small; this is not surprising, since no bond needs to be broken for a such change and no change in conformation is

required. We also observe from this symmetry analysis that the water molecule can move on the face OE1, OE2, OB4, and OB1, with two preferential asymmetric positions in which the water oxygen is in prismatic positions and an intermediate position with the water oxygen in a capping position.

Rotational correlation times: The rotational correlation time of the complex strongly influences the relaxivity.[25] It describes how fast the complex tumbles in solution. One way to improve the relaxivity of new contrast agents is to increase their rotation correlation time and their chemical water exchange rate. From molecular dynamics simulation trajectories it is possible to calculate the second-order rotational correlation time, relevant for NMR spectroscopy, from the rotational correlation function of a given vector.[26] This vector can be defined by two atoms, or a group of atoms, letting us calculate the global molecular tumbling rate as well as the local tumbling rate of one atom around the metal ion, for example.

From the NMR technique we obtain the second-order rotational correlation time τ_R.[3] One hypothesis commonly adopted for the experimental data analysis is that the complex is rigid and isotropic. It implies that one unique rotational correlation time is used to describe the tumbling of all vectors in the complex.[27] Nevertheless it has been shown very recently experimentally that the protons of the coordinated water molecule tumble faster than the oxygen, because they have more degrees of freedom than the oxygen atoms.[28] The influence of internal motions on nuclear spin relaxation is known problem in NMR spectroscopy. For example, the rotational contribution to the relaxivity of macromolecular MRI contrast agents is divided into global and local rotational correlation times, in order to separate the macromolecular rotation from the local tumbling of the chelating site, by using the Lipari – Szabo approach.[29]

We present in Table 9 the second-order rotational correlation times calculated on the first 457 ps of MD-A on the following vectors: 1) the sum of vectors Gd–OB1, Gd–OE1, Gd–OE2 and Gd–OB4, representing $\tau_R([Gd(egta)(H_2O)]^-)$, 2) vector Gd–OWC, 3) vector Gd–1HWC, and 4) vector Gd–-2HWC. τ_R(Gd–OWC) is close to the value of $\tau_R([Gd(egta)(H_2O)]^-)$, with a value that is only 5% lower than the complex one. This is not a surprise, since the inner sphere water oxygen is a part of the coordination polyhedron and, consequently, can be considered nearly rigidly bound. On Figure 8, one clearly observes that preferential positions are adopted by the two water hydrogen atoms, due to electrostatic interactions with surrounding atoms. Interaction of 1HWC with OE2 is stronger than interaction of 2HWC with OB4, as proved by the higher probability of 1HWC to be close to OE2. This explains the 30% difference in τ_R between the two protons. ^{1}H NMR spectroscopy does not discriminate the two protons, so one can only measure an average τ_R. An average value of 30.6 ps for τ_R(Gd–HWC) will be used for this discussion. The protons of the inner sphere water molecule tumble faster than the global complex, as proved by the ratio τ_R(Gd–HWC):$\tau_R([Gd(egta)(H_2O)]^-)$ of about 72%. Even if the calculated values should be taken as qualitative, this indicate that a differentiation between τ_R(complex) and τ_R(protons) could be necessary in future analysis. The unique experimental rotational correlation time obtained as mentioned above is in excellent agreement with the different correlation times calculated from the simulations.

Table 9. Second-order rotational correlation times calculated on different vectors.

Vector studied	τ_R [ps]
$[Gd(egta)(H_2O)]^-$	42.8 ± 0.1
Gd–OWC	40.5 ± 0.1
Gd–1HWC	35.2 ± 0.1
Gd–2HWC	26.0 ± 0.1
exptl[3]	58 ± 6

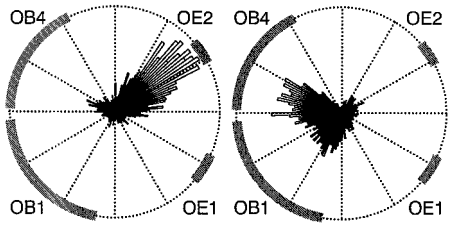

Figure 8. Distribution of the dihedral angle (OE1 + OE2)/2-Gd-OWC-X in MD-A, with X = 1HWC (left) and 2HWC (right). Gray zones mark angle domain of the surrounding coordination sites labeled as X = OB1, OE1, OE2, and OB4. The radius of the distribution is proportional to the probability of the dihedral angle.

Conclusion

Molecular dynamics simulations have been performed on a Gd^{3+} poly(amino carboxylate) complex without any artificial constraints on the first coordination sphere, such as Gd–coordination-site covalent bond or so. This, to our knowledge, has never been done before. From these simulations using new X-ray solid-state molecular structures, a study of the complex in solution has been carried out especially focused on the internal behavior of the complex. Changes in the coordination of the Gd^{3+} were observed, with the departure of the inner sphere water molecule, and volume profiles for the reaction of dissociation has been calculated, corroborating the experimental values obtained in a previous paper.[3] Changes in the conformation of the complex, with the flips of some dihedral angles, very fast changes in the symmetry orientation of the coordination polyhedron and steric constraints of the ligand $egta^{4-}$ on the inner sphere water molecule are related with the chemical water exchange rate. These very fast fluctuations of the inner sphere are also related to the transient zero-field splitting (ZFS) modulation correlation time, τ_v. From the simulations we obtain one change in symmetry every 2.2 ps. This value is similar to the τ_v values obtained for $[Gd(dota)(H_2O)]^-$ (0.54 ps), $[Gd(dtpa)(H_2O)]^{2-}$ (1.33 ps), and [Gd(dtpa-bma)(H_2O)] (1.07 ps).[1, 2] Unfortunately the experimental data analysis for $[Gd(egta)(H_2O)]^-$ was performed without separating the static ZFS (modulated by rotation) and the transient ZFS contributions. The reported value (24 ps) is therefore a mixture of $\tau_R([Gd(egta)(H_2O)]^-)$ and the actual τ_v. This

0947-6539/02/0805-1038 $ 17.50+.50/0 *Chem. Eur. J.* **2002**, *8*, No. 5

relation between the fast changes in symmetry orientation and τ_v lets us propose, for the first time, a molecular mechanism for the electronic relaxation of this complex.

A discrimination between the global complex, the Gd–OW and the two Gd–HW rotational correlation times let us propose a revision of one of the hypotheses used in the experimental NMR and EPR data treatment: in the case of $[Gd(egta)(H_2O)]^-$, the complex is not rigid and the ratio $\tau_R(Gd–HW):\tau_R([Gd(egta)(H_2O)]^-)$ is about 72%, and the ratio $\tau_R(Gd–OW):\tau_R([Gd(egta)(H_2O)]^-)$ is about 95%. If the values of τ_R gives similar ratios for other poly(amino carboxylate) complexes, one should differentiate them in the future global NMR/EPR data analysis treatment. The value of τ_R used to describe ^{17}O NMR and EPR data can be taken as the same, according to the great similitude of $\tau_R([Gd(egta)(H_2O)]^-)$ and $\tau_R(Gd–OW)$. The value of $\tau_R(Gd–HW)$ should be taken at 75% of the value of $\tau_R(Gd–OW)$ when simultaneously fitting ^{17}O NMR and NMRD data.

To increase the water exchange rate on the Gd^{3+} in order to increase the proton relaxivity, one has to synthesize complexes in which the distance Gd–OW is as long as possible, like in the $egta^{4-}$ complex. The fact than the inner sphere water molecule can stay in two positions on the complex might also be favorable for a high water exchange rate.

The use of molecular dynamics simulations provides us with a valuable probe of the molecular mechanisms underlying the experimental behavior in solution. Future investigations on other Gd^{3+} poly(amino carboxylate) complexes by using molecular dynamics simulations will allow us to establish correlations between the microscopic instantaneous phenomena and the macroscopic time averaged observables.

Acknowledgements

We thank Prof. Dieter Schwarzenbach for helpful discussions on symmetry analysis, Dr. Alain Porquet for providing a very efficient program of analysis, KERUBIN, and Dr. Alain Borel for helpful discussions about molecular dynamics. This work was supported by a Novartis grant, the Swiss National Science Foundation and the Swiss OFES as part of the European COST Actions D9 "Advanced Computational Chemistry of Increasing Complex Systems" and D18 "Lanthanide Chemistry for Diagnosis and Therapy". M.B. and K.I.H. thank NATO Science Program for a travel grant.

[1] R. B. Lauffer, *Chem. Rev.* **1987**, *87*, 901–927.
[2] P. Caravan, J. J. Ellison, T. J. McMurry, R. B. Lauffer, *Chem. Rev.* **1999**, *99*, 2293–2352.
[3] S. Aime, A. Barge, A. Borel, M. Botta, S. Chemerisov, A. E. Merbach, U. Müller, D. Pubanz, *Inorg. Chem.* **1997**, *36*, 5104–5112.
[4] T.-Z. Jin, S.-F. Zhao, G.-X. Xu, Y.-Z. Han, N.-C. Shi, Z.-S. Ma, H. Xuebao, *Acta Chim. Sin.* **1991**, *49*, 569–575.
[5] C. A. Chang, L. C. Francesconi, M. F. Malley, K. Kumar, J. Z. Gougoutas, M. F. Tweedle, D. W. Lee, L. J. Wilson, *Inorg. Chem.* **1993**, *32*, 3501–3508.
[6] R. Ruloff, T.Gelbrich, J. Sieber, E. Hayer, L.Beyer, *Z. Naturforsch. Teil B* **1997**, *52*, 805–809.
[7] D.Chen, P. J. Squattrito, A. E. Martell, A.Clearfield, *Inorg. Chem.* **1990**, *29*, 4366–4368.
[8] SHELXTL/PC V5.03, Bruker AXS, Madison, WI (USA).
[9] A. J. C. Wilson, *International Tables for X-ray Crystallography*, *Vol. C*, Kluwer Academic Publishers, Dordrecht, **1992**, Tables 6.1.1.4 (pp. 500–502) and 4.2.6.8 (pp. 219–222).
[10] D. A. Case, D. A. Pearlman, J. W. Caldwell, T. E. Cheatham , W. S. Ross, C. L. Simmerling, T. A. Darden, K. M. Merz, R. V. Stanton, A. L. Cheng, J. J. Vincent, M. Crowley, V. Tsui, R. J. Radmer, Y.Duan, J. Pitera, I. Massova, G. L. Seibel, U. C. Singh, P. K. Weiner and P. A. Kollman, AMBER 6.0, University of California, San Francisco (USA), **1999**.
[11] a) S. J. Weiner, P. A. Kollman, D. A. Case, U. C. Singh, C. Ghio, G. Alagona, S. Profeta, Jr, P. Weiner,. *J. Am. Chem. Soc.* **1984**, *106*, 765; b) S. J. Weiner, P. A. Kollman, D. T. Nguyen, D. A. Case, *J. Comput. Chem.* **1986**, *7*, 230.
[12] M. J. Frisch, G. W. Trucks, H. B. Schlegel, G. E. Scuseria, M. A. Robb, J. R. Cheeseman, V. G. Zakrzewski, J. A. Montgomery, R. E. Stratmann, J. C. Burant, S. Dapprich, J. M. Millam, A. D. Daniels, K. N. Kudin, M. C. Strain, O. Farkas, J. Tomasi, V. Barone, M. Cossi, R. Cammi, B. Mennucci, C. Pomelli, C. Adamo, S. Clifford, J. Ochterski, G. A. Petersson, P. Y. Ayala, Q. Cui, K. Morokuma, D. K. Malick, A. D. Rabuck, K. Raghavachari, J. B. Foresman, J. Cioslowski, J. V. Ortiz, B. B. Stefanov, G. Liu, A. Liashenko, P. Piskorz, I. Komaromi, R. Gomperts, R. L. Martin, D. J. Fox, T. Keith, M. A. Al-Laham, C. Y. Peng, A. Nanayakkara, C. Gonzalez, M. Challacombe, P. M. W. Gill, B. G. Johnson, W. Chen, M. W. Wong, J. L. Andres, M. Head-Gordon, E. S. Replogle, J. A. Pople, Gaussian 98 (Revision A.5), Gaussian, Inc., Pittsburgh PA, **1998**.
[13] B. H. Besler, K. M. J. Merz, P. A. Kollmann, *J. Comput. Chem*. **1990**, *11*, 431–439.
[14] M. Dolg, H. Stoll, A. Savin, H. Preuss, *Theor. Chim. Acta* **1989**, *75*, 173–194.
[15] A. Borel, L. Helm, A. E. Merbach, *Chem. Eur. J.* **2001**, *7*, 600–610.
[16] W. L. Jorgensen, J. Chandrasekhar, J. D. Madura, *J. Chem. Phys.* **1983**, *79*, 926–935.
[17] A.Porquet, KERUBIN 4.4.9, Institute of Inorganic and Analytical Chemistry, University of Lausanne (Switzerland), **2000**.
[18] Matlab 5.3.1, The Mathworks, Inc. Natick, MA (USA), **1999**.
[19] a) F.Yerly, VISUALISEUR 2.2.4, Institute of Inorganic and Analytical Chemistry, University of Lausanne (Switzerland), **1999**; b) F.Yerly, OPTIMISEUR 2.2.1, Institute of Inorganic and Analytical Chemistry, University of Lausanne (Switzerland), **1999**.
[20] M. L. Connolly, *Science* **1983**, *221*, 709–713.
[21] Cerius^2 v.3.0, Molecular Simulations, Cambridge (UK).
[22] T. Kowall, F. Foglia, L. Helm, A. E. Merbach, *Chem. Eur. J.* **1996**, *2*, 285–294.
[23] D. L. Kepert, *Inorganic Stereochemistry (Inorganic Chemistry Concepts 6)*, Springer, Berlin, **1982**, Chapters 12 and 13.
[24] C. K. Schauer, O. P. Anderson *J. Chem. Soc. Dalton Trans.* **1989**, 185–191.
[25] D. H. Powell, O. M. Ni Dhubhghaill, D. Pubanz, L. Helm, Y. S. Lebedev, W. Schlaepfer, A.E Merbach *J. Am. Chem. Soc*. **1996**, *118*, 9333–9346.
[26] R. W. Impey, P. A. Madden, I. R. McDonald, *Mol. Phys.* **1982**, *46*, 513–539.
[27] S. Rast, A. Borel, L. Helm, E. Belorizky, P. H. Fries, A. E. Merbach, *J. Am. Chem. Soc.* **2001**, *123*, 2637–2644.
[28] F. A. Dunand, A. Borel, A. E. Merbach, *J. Am. Chem. Soc.*, in press.
[29] F. A. Dunand, E. Tóth, R. Hollister, A. E. Merbach, *J. Biol. Inorg. Chem.* **2001**, *6*, 247–255.
[30] S. Rast, P. H. Fries, E. Belorizky *J. Chem. Phys.* **2000**, *113*, 8724–8735.
[31] S. Rast, A. Borel, L. Helm, E. Belorizky, P. H. Fries, A. E. Merbach *J. Am. Chem. Soc.* **2001**, *123*, 2637–2644.

Received: September 5, 2001 [F3532]